

Article

Study on Sustainable Application of Low-Carbon Supersulfated Cement with Alkanolamines

Runduo Zhou ¹, Bingxin Jin ¹, Shuanglei Wu ¹, Shujing Fan ², Fafu Hang ² and Huxing Chen ^{1,*}

¹ School of Materials Science and Engineering, Zhejiang University, Hangzhou 310027, China

² Linhai Zhongxin New Building Materials Co., Ltd., Taizhou 317000, China; liuluorenjiantree@163.com (S.F.)

* Correspondence: chenhx@zju.edu.cn

Abstract: As an environmentally friendly cement material in green buildings, due to its low contribution to air pollution and its substantial use of solid waste, supersulfated cement (SSC) has been extensively studied. However, the low early strength of sustainably utilized SSC needs to be addressed. In order to use SSC to achieve great reductions in energy consumption during industrial production, the effects of triethanolamine (TEA), diethanolisopropanolamine (DEIPA) and triisopropanolamine (TIPA) (with dosages ranging from 0.02% to 0.08%) on the strength and hydration of SSC were studied, and the underlying mechanism was analyzed by TGA, XRD and SEM. The results show that TEA and DEIPA significantly improve the 3-day and 28-day strength of SSC. The former is better at low dosages, while the latter is more suitable for high dosages. TIPA also enhances the 3-day strength of SSC, but it is not as good as the other two alkanolamines. The chelation of alkanolamine with Al^{3+} ions plays an important role in the strength development of SSC, which accelerates the decomposition of slag and the formation of ettringite. In summary, adding alkanolamines to low-carbon cement systems with a high proportion of industrial by-products such as SSC is a potential and effective solution. In addition, alkanolamines can be used as a strength promoter for most low-carbon blends, which fully utilize solid waste.



Citation: Zhou, R.; Jin, B.; Wu, S.; Fan, S.; Hang, F.; Chen, H. Study on Sustainable Application of Low-Carbon Supersulfated Cement with Alkanolamines. *Sustainability* **2024**, *16*, 3008. <https://doi.org/10.3390/su16073008>

Academic Editor: José Ignacio Alvarez

Received: 30 January 2024

Revised: 23 March 2024

Accepted: 2 April 2024

Published: 4 April 2024



Copyright: © 2024 by the authors. Licensee MDPI, Basel, Switzerland. This article is an open access article distributed under the terms and conditions of the Creative Commons Attribution (CC BY) license (<https://creativecommons.org/licenses/by/4.0/>).

1. Introduction

Cement production is the most energy-consuming and unsustainable process in the building materials industry. For example, Chinese cement production has reached 2.4 billion tons, resulting in 1.23 billion tons of carbon emissions, which accounts for approximately 13% of the country's total carbon emissions. This phenomenon has caused the Chinese cement industry to face severe challenges in terms of air pollution and unsustainable development.

In recent years, with the deepening of the concept of environmental protection [1–5], more attention has been paid to the use of solid waste like industrial by-products. Many studies have shown that alkanolamine better improves the mechanical properties of low-carbon cement containing solid waste than ordinary Portland cement (OPC) [6,7]. Alkanolamines, including triethanolamine (TEA), triisopropanolamine (TIPA), diethanolisopropanolamine (DEIPA), and ethyldiisopropylamine (EDIPA), which are widely used in the cement industry as grinding aids, significantly influence the hydration and strength properties of cement. TEA promotes the early strength of OPC at low content but is harmful to the strength of cement-based materials at high content, especially in terms of late strength [8–10]. The good early mechanical properties are because TEA promotes the dissolution of C_3A and C_4AF and the hydration of $\text{C}_3\text{A} + \text{gypsum}$, which accelerates the formation of ettringite [11–13] and the secondary hydration of C_3A in OPC [8,9,14], related to the complexation of TEA with Ca^{2+} , Al^{3+} and Fe^{4+} ions in solution [9,15,16]. The

low late strength arises due to the inhibition of the hydration of C₃S by TEA [7,9,10,17]. In contrast to TEA, TIPA promotes the late strength of OPC, but its effect on the early strength is slight [8,9,18,19]. The high late strength is because TIPA has a continuous effect on the dissolution of ferrite, increasing the concentrations of Fe³⁺ and Al³⁺ ions in pore solution, and this process accelerates the consumption of CH, thus promoting the formation of AFt or AFm [20–22]. DEIPA and EDIPA are new alkanolamines similar to the above two alkanolamines. Wang et al. [23] reported that alkanolamines with asymmetric molecular structure have stronger solubilizing ability than alkanolamines with symmetric molecular structure. DEIPA and EDIPA show better late strength than TEA and better early strength than TIPA when used in OPC [9]. The addition of the two alkanolamines to OPC promotes the initial dissolution of C₃A and C₄AF [24,25] and accelerates the secondary hydration of C₃A and the conversion of AFt to AFm [8,26,27]. Both DEIPA and EDIPA increase the hydration degree of C₃S at late stage [9,25,26]. Because alkanolamine accelerates the dissolution of Al³⁺ and Fe⁴⁺ ions in supplementary cementitious materials (SCMs) and enhances the pozzolanic reaction, its promotion on blended cements is better than its promotion on OPC [6,20,28]. Different views on whether alkanolamines directly promote SCMs have been discussed. Kong et al. [7] believed that the influence of TEA on the pozzolanic reaction of FA can consume more CH, resulting in a lower CH content in FAC; the reduction in actinomorphic CH is conducive to the refinement of pore structure [10]. Riding et al. [29] showed that DEIPA can directly act on slag by measuring the heat of hydration of cement and cement-slag blend. However, Ma et al. [21] believed that the addition of TIPA first accelerates the hydration of cement and generates more CH, which further stimulates the pozzolanic reaction of FA and consumes more CH.

At present, alkanolamines have been extensively studied in many environmentally friendly blended cement systems that replace approximately only 30 wt.% of clinker, but few scholars have focused on systems with higher clinker replacement levels.

Supersulfated cement (SSC) is a low-carbon system with a small amount of clinker. The proportion of clinker replacement is generally approximately 90 wt.%, of which the proportion of granulated blast furnace slag (GBFS) is usually greater than 80 wt.%, and the proportion of gypsum is approximately 10–20 wt.% [30–33]. Sometimes, a small amount of alkali activator, such as KOH [34,35], is used instead of clinker to contribute to the alkali excitation of slag. The main hydration products of SSC are ettringite and C-S-H gel [36,37]. The clinker dissolves and generates CH at the beginning of hydration, giving the environment a high alkalinity level to encourage the slag to dissolve [38]. The dissolved Al³⁺, Ca²⁺ and Si⁴⁺ ions in GBFS react with calcium sulfate (CS) to form ettringite (C₆AS₃H₃₂) at early stage, and calcium silicate hydrate (C-S-H) phase in later stages to support the increase in strength [32,39]. The simplified hydration process of SSC is demonstrated in Equation (1) [38].



Although SSC has the advantages of good durability [39–42], low heat of hydration [36], good workability and rheology [43], it also has the disadvantages of low early strength and weak carbonization resistance.

When used as a low-air-pollution material in construction engineering, SSC has the shortcomings of low early strength. SSC is a hydration system dominated by aluminum mineral phase at early stage. Moreover, most alkanolamines are early hydration promoters of cement and can complex Ca²⁺, Al³⁺ and Fe⁴⁺ ions in pore solution to accelerate the hydration of aluminate and ferrite. Therefore, this study investigated whether alkanolamines had a beneficial effect on SSC hydration. In addition, we evaluated whether alkanolamine had a similar or more pronounced hydration mechanism in SSC than in OPC.

Therefore, this study attempted to add alkanolamine to SSC for the first time to explore the effect of alkanolamine on the hydration and mechanical properties of such a low-early-strength cement system with ettringite as the main mineral phase. A comparative study on three alkanolamines (TEA, DEIPA and TIPA) was conducted. Due to its high toxicity,

EDIPA was not considered. This not only has a guiding significance for the exploration of the general law of alkanolamine in the cement system containing SCMs, but also provides a new reference and idea for the development of new low-carbon environmental protection cement and the utilization of solid waste such as slag.

2. Materials and Methods

2.1. Materials

Portland cement clinker, desulfurization gypsum, ground granulated blast furnace slag (GGBS) and three kinds of alkanolamines were used in this experiment. The clinker was obtained from South Cement Co., Ltd., Hangzhou, China. Desulfurization gypsum was from Xindu Cement Co., Ltd., Hangzhou, China. GGBS (grade S95) was obtained from Dehang Mining Products Co., Ltd., Shijiazhuang, China. The density and specific surface area of GGBS were 3.1 g/cm^3 and $429\text{ m}^2/\text{kg}$, respectively. The chemical compositions of these materials are shown in Table 1. Figure 1 shows the SEM morphologies of GGBS and desulfurization gypsum. The slag is angular and granular, while the gypsum has a parallelepiped shape. TEA (Yien Chemical Technology Co., Ltd., Shanghai, China, 98% purity), TIPA (Yien Chemical Technology Co., Ltd., Shanghai, China, 95% purity) and DEIPA (ShengHong Holding Group Co., Ltd., Suzhou, China, 85% purity) were used, and their molecular formulas are shown in Figure 2.

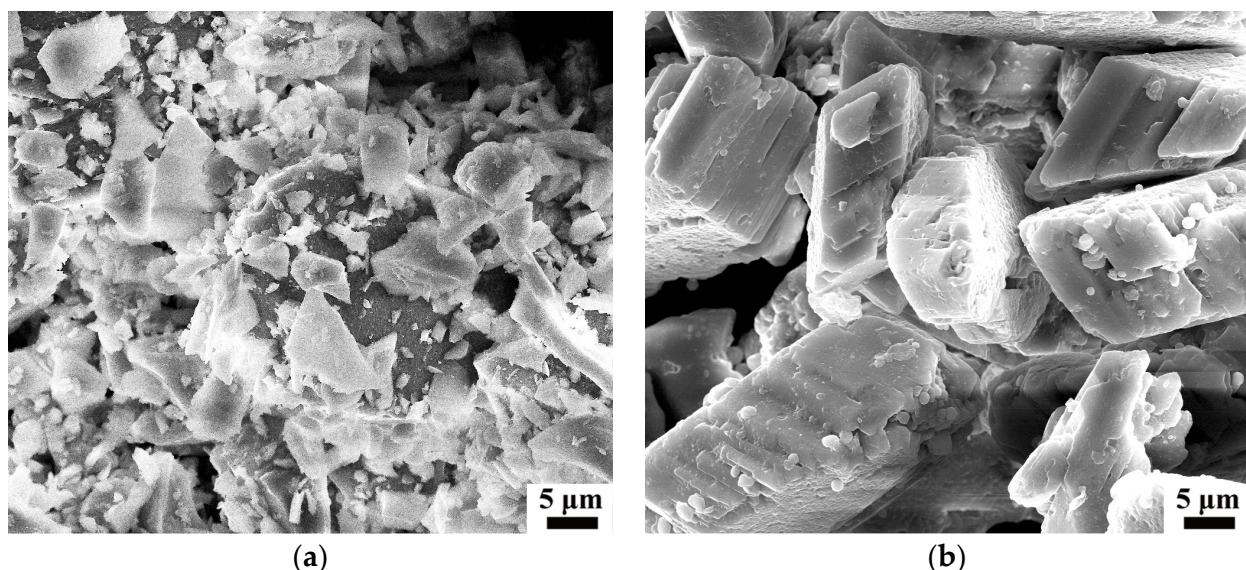


Figure 1. SEM images of the raw materials: (a) GGBS; (b) Gypsum.

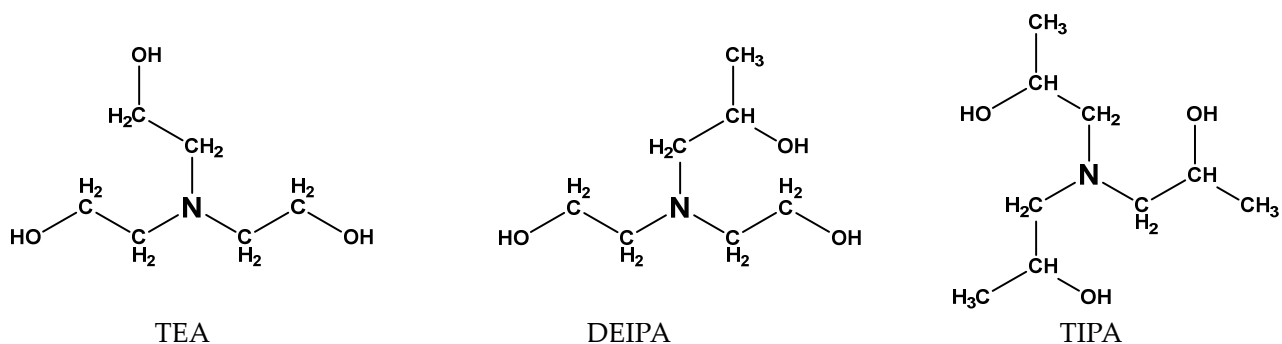


Figure 2. Molecular formulas of TEA, DEIPA and TIPA.

Table 1. Chemical compositions of raw materials (wt.%).

	SiO_2	Al_2O_3	Fe_2O_3	CaO	MgO	SO_3	Loss
Cement	22.16	5.18	3.95	66.25	1.26	0.36	0.09
GGBS	34.5	17.7	1.03	34	6.01	1.64	0.84
Desulfurization gypsum	2.18	0.91	0.49	30.07	0.25	42.38	22.71

2.2. Mix Proportion

The clinker was first ground with a 200-mesh sieve in a standard small mill of $\Phi 500$ until the residue content was less than 6.0%. Various SSC binders were prepared by mixing clinker, desulfurization gypsum and GGBS. The basic ratio of SSC was 80 wt.% slag, 15 wt.% desulfurization gypsum and 5 wt.% clinker. The proportions of alkanolamine added to SSC were 0, 0.02%, 0.04%, 0.06% and 0.08%. Different mixtures are indicated by corresponding symbols for the convenience of the discussion below, as shown in Table 2. After proportional matching, the specimens were mixed uniformly by stirring.

Table 2. Mixture design of SSC cement (wt.%).

ID	SSC	TEA	DEIPA	TIPA
Blank	100	0	0	0
TEA0.02	100	0.02	0	0
TEA0.04	100	0.04	0	0
TEA0.06	100	0.06	0	0
TEA0.08	100	0.08	0	0
DEIPA0.02	100	0	0.02	0
DEIPA0.04	100	0	0.04	0
DEIPA0.06	100	0	0.06	0
DEIPA0.08	100	0	0.08	0
TIPA0.02	100	0	0	0.02
TIPA0.04	100	0	0	0.04
TIPA0.06	100	0	0	0.06
TIPA0.08	100	0	0	0.08

2.3. Methodology

2.3.1. Mechanical Strength

Alkanolamine was dissolved in water in advance and the solution was then mixed with the binder to prepare the paste with a w/c of 0.4. The pastes were stirred in a laboratory mixer at a speed of 140 r/min for 120 s, stopped mixing for 15 s, and then stirred at a speed of 285 r/min for 120 s. The equipment used in this process was a NJ-160A cement paste mixer from Luda Experiment Instrument Co., Ltd., Shanghai, China. The fresh pastes were poured into 20 mm \times 20 mm \times 20 mm mold. All of mold were stored in a curing box with a humidity of more than 95% and a temperature of $(20 \pm 1)^\circ\text{C}$ for 24 h. The equipment used was an HBY-40B cement (concrete) constant-temperature and humidity cabinet from Luda Experiment Instrument Co., Ltd., Shanghai, China. Then, the specimens were demoulded and further cured in water at $(20 \pm 1)^\circ\text{C}$ by using an HBY-30 constant-temperature water cabinet from Luda Experiment Instrument Co., Ltd., Shanghai, China. The hardened pastes that were cured for 3 days and 28 days were tested for compressive strength at a rate of 0.2 kN/s by using a YZH-300·10 constant load cement flexural compression testing machine from Luda Machinery Instrument Co., Ltd., Shaoxing, China. The average compressive strength of six specimens was adopted.

After the compressive strength test, the hydration was stopped by submerging small pieces of samples in alcohol. The pieces were then dried in an oven at 40°C for 1 d and grounded to pass through the sieve with 80 μm for XRD, TGA and SEM analysis.

2.3.2. Isothermal Calorimetry

The heat of hydration of the SSC pastes after the addition of TEA, DEIPA or TIPA was measured by a TAM Air isothermal calorimeter from TA Company (New Castle, DE, USA) at 20 °C for 3 days using external stirring method [15]. An amount of 10 g of dry cement was loaded in glass ampoules, and syringes were loaded with 5 g of alkanolamine–water solution. After reaching a steady baseline, the solution was injected into the ampoule and mixed with the cement. The dosages of alkanolamines were 0.08%.

2.3.3. XRD and QXRD

The phase composition was investigated using a Rigaku Ultimate IV powder X-ray CuK α ($\lambda = 1.5418 \text{ \AA}$) radiation diffractometer operated at 40 kV and 40 mA. Data were collected from 5° to 65° at 5°/min. Before testing, samples stored in ethanol were ground and dried at 40 °C for 24 h. Quantitative X-ray diffraction (QXRD) analysis utilized the Rietveld method in X'Pert HighScore Plus (version 3.0e) using the external standard method, with rutile as the standard reference. All structure models used for Rietveld refinement are shown in Table 3.

Table 3. Structure models used for Rietveld refinement.

Phase	Formula	Crystal System	ICSD Cods	Reference
Ettringite	3CaO·Al ₂ O ₃ ·3CaSO ₄ ·32H ₂ O	Trigonal	155395	[44]
Gypsum	CaSO ₄ ·2H ₂ O	Monoclinic	409581	[45]
Calcite	CaCO ₃	Trigonal	40545	[46]
Rutile (standard)	TiO ₂	Tetragonal	202241	[47]

2.3.4. TGA

TGA was conducted with a TGA/DSC3+ synchronous thermal analyzer from Mettler, Zurich, Switzerland. The samples were heated from 50 to 1000 °C at a rate of 10 °C/min under a 30 mL/min flow of N₂. The preparation process of powder samples used for testing was consistent with that for XRD analysis.

2.3.5. Degree of Hydration

The selective dissolution of the hydrate phases in ethylenediaminetetraacetic acid (EDTA) described by Kocaba et al. [48] was used to evaluate the reaction degree of slag. This method is usually used for blended pastes. The preparation of powder samples used for testing was consistent with that of XRD samples. The hydration degree of slag was calculated by referring to Equation (2) recommended by Luke et al. [49]:

$$\alpha_{\text{SLAG}} = 100 - \left(\frac{w_2 + (f_{\text{SLAG}}(1 - R_{\text{GGBS}})w_1) - (f_{\text{CEMENT}}C_r w_1)}{f_{\text{SLAG}}w_1} \cdot 100 \right) \quad (2)$$

where w_1 is the weight of sample (ignited weight), w_2 is the weight of residue (105 °C dry weight), C_r is the percentage of cement residue divided by 100, f_{SLAG} is the percentage of initial slag in the blended cement, f_{CEMENT} is the percentage of initial cement in the blended cement, and R_{GGBS} is the percentage of unreacted slag that is insoluble in EDTA.

In addition, any method is subject to a certain amount of error. The EDTA selective dissolution method is not an accurate method. However, it could still be used as a reference to assist analysis.

2.3.6. SEM

The morphology of SSC pastes was observed by field emission environmental scanning electron microscopy (SEM; FEG650, FEI, Shanghai, China). The acceleration voltage was 20 kV. Before the test, the sample was coated with a thin gold layer.

3. Results

3.1. Mechanical Properties

The compressive strength of SSC specimens after the addition of different dosages of alkanolamines is shown in Figure 3. Detailed compressive strength data is listed in Tables S1–S7 of Supplementary Materials. At 3 days, TEA and DEIPA significantly improve the mechanical properties of SSC. Compared with that of DEIPA, the performance of TEA is superior at 3-day strength, while the improvement in SSC caused by TIPA is relatively slight. The strength of SSC increases obviously with the addition of TEA, especially at low dosages. When 0.02% TEA is added, the strength increases by 4.1 MPa. When increasing the dosage to 0.06% TEA, the strength reaches a maximum value and increases by 8.3 MPa compared with that of the blank sample. When 0.02% DEIPA is added, the strength increases by only 2.3 MPa, and when 0.04% DEIPA is added, the strength increases by only 4.4 MPa. However, at relatively high dosages, DEIPA is better than TEA. When the dosage reaches 0.08%, the strength of SSC with DEIPA increases by 10.5 MPa, while the strength of the SSC with TEA increases by only 7.9 MPa. TIPA slightly increases the strength of SSC only at high dosages, and the strength increase is lower than that of the other two alkanolamines. At a dosage of 0.02%, TIPA decreases the strength by 0.1 MPa, and it increases the strength by only 2.9 MPa at a dosage of 0.08%.

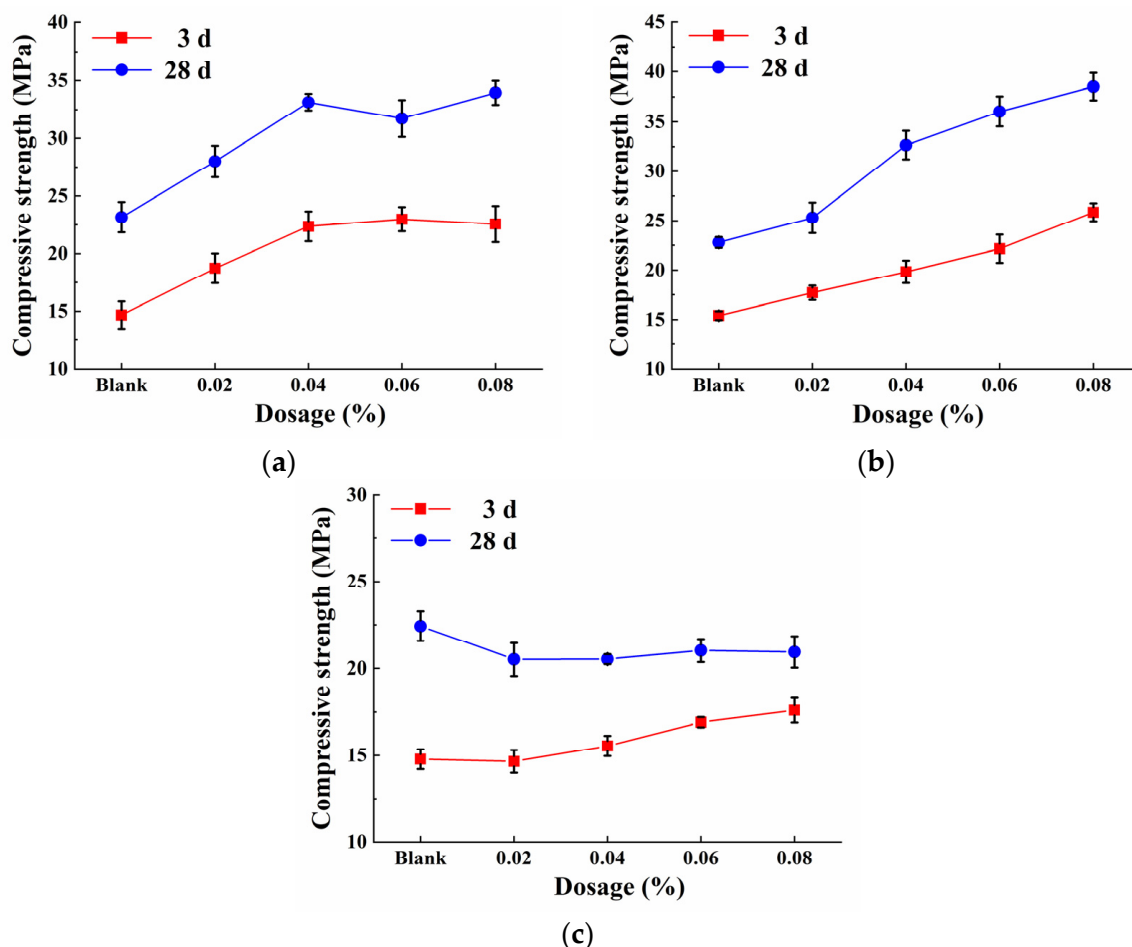


Figure 3. Influences of alkanolamines on the compressive strength of SSC pastes with different dosages: (a) TEA; (b) DEIPA; (c) TIPA.

At 28 days, TEA and DEIPA still increase the strength of SSC, but the two alkanolamines are different. The strength of SSC with TIPA generally decreases at all dosages. TEA significantly enhances the strength of SSC at low dosages, but its strength fluctuates

and even decreases with increasing dosage. The effect of TEA on the strength of SSC is different from that of OPC. At a dosage of 0.04%, the strength with TEA is 33.1 MPa, and when the dosage reaches 0.06%, the strength is 31.7 MPa, which is 1.4 MPa lower than the previous one. The strength of SSC is still enhanced with the increasing dosage of DEIPA. The strength after adding 0.08% DEIPA is 38.5 MPa, which is 15.7 MPa higher than that of the blank sample; this result is similar to that described by Xu et al. [9]. With the addition of 0.08% TIPA, the strength of SSC is 21.0 MPa, which is 1.4 MPa lower than that of the blank sample; this result is also different from OPC [9].

3.2. Degree of Slag Hydration

The selective dissolution method of EDTA described by Luke et al. [49] can be used to measure the hydration degree of slag. Prior to testing the SSC mixtures, it has shown that 96% of unhydrated slag is insoluble during EDTA extraction.

The hydration degree of slag with different dosages of TEA, DEIPA and TIPA at 3 days and 28 days is shown in Figure 4. Detailed hydration degree data is listed in Table S8 of Supplementary Materials. At 3 days, the hydration degree is improved with the increasing dosage of TEA and DEIPA. A high degree of hydration is achieved at a low dosage of TEA, which is in good agreement with strength. But at high dosages, the hydration degree with the addition of DEIPA is greater than that with TEA. TIPA slightly increases the hydration degree of slag at 3 days. At 28 days, the hydration degree after adding DEIPA is better than that after adding TEA on the whole. Only at a dosage of 0.02% is the influence of DEIPA slightly lower than that of TEA. However, the hydration degree of slag adding TIPA is still weak at 28 days.

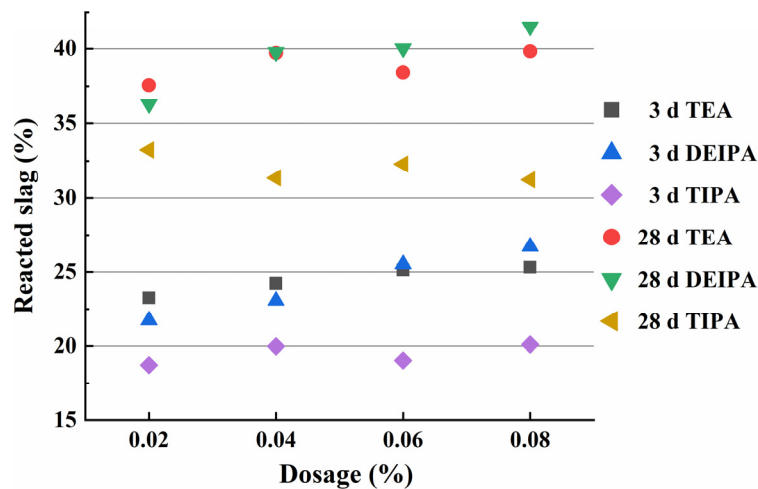


Figure 4. Influence of alkanolamines with different dosages on the hydration degree of slag in SSC at 3 days and 28 days.

3.3. Heat Evolution

Isothermal calorimetry was used to test the evolution curves for SSC after the addition of TEA, DEIPA and TIPA for up to 72 h. The hydration rate and cumulative heat results are shown in Figure 5. Detailed hydration rate data is listed in Table S9 of Supplementary Materials and high-resolution pictures are shown in Figures S1 and S2. To clearly quantify and compare the differences between the hydration curves of each group, some characteristic parameters on the heat evolution curve are extracted and labeled as A, B and C, as shown in Table 4. t_A and $(dQ/dt)_A$ represent the ending time and heat generation rate of induction period, respectively. k_B represents the secant slope on the heat evolution curve between A and C and it indicates the maximum acceleration rate of hydration. t_C and $(dQ/dt)_C$ represent the maximum heat generation rate time and the maximum heat generation rate of the main hydration peak, respectively. Q is the cumulative heat of hydration.

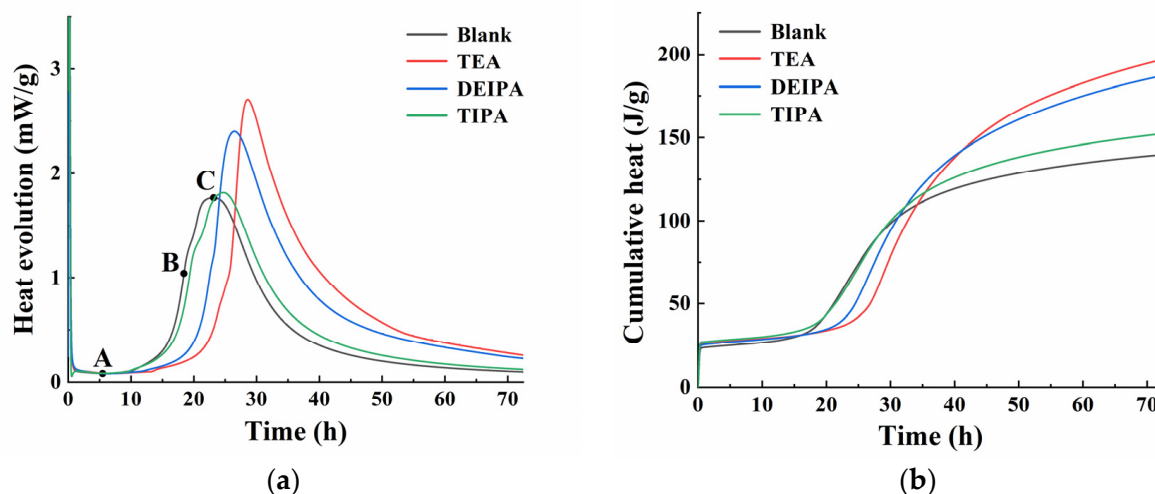


Figure 5. Hydration heat of the SSC pastes with or without alkanolamines: (a) Hydration rate; (b) Cumulative heat (A: Ending time of induction period. B: The maximum secant slope on the heat evolution curve between A and C. C: The maximum heat generation rate time).

Table 4. The effects of alkanolamines on the characteristic parameters of cement hydration.

	t_A (h)	$(dQ/dt)_A$ (mW/g)	t_C (h)	$(dQ/dt)_C$ (mW/g)	Q (J/g)	k_B
Blank	5.5	0.08119	23.18333	1.76642	139.89844	0.42955
TEA	7.56667	0.08109	28.66667	2.70791	196.85867	0.89248
DEIPA	6.35833	0.07967	26.49167	2.4025	187.21136	0.68707
TIPA	5.96667	0.08271	24.71667	1.81567	152.32699	0.39886

The general heat flow curve of OPC is divided into five stages: initial reaction, induction, acceleratory and deceleratory periods, and the final period of slow reaction. The curve has four characteristic peaks [10,50]. However, in SSC, the curve is generally divided into three stages: initial wetting and dissolution peak, dormant period with low heat release rate and wide exothermic peak [37,51].

According to Figure 5a, with the addition of alkanolamines, the main hydration peak is more or less delayed to the right. By comparing the difference of t_C in Table 4, the strength of the delaying effect of alkanolamine on the main hydration peak of SSC is compared as follows: TEA > DEIPA > TIPA. TEA and DEIPA significantly delay the hydration peak of SSC, while TIPA is relatively weak. The regularities satisfied by t_A also indicate a delay in hydration.

However, the addition of these three alkanolamines increases the maximum heat generation rate of the main hydration peak. For $(dQ/dt)_C$: TEA > DEIPA > TIPA. TEA and DEIPA greatly promote the peak strength of the main hydration peak, while the maximum heat generation rate of TIPA is close to that of the blank sample. The law satisfied by k_B also indicates the increase in peak strength. The delay of the main hydration peak is consistent with the increase in the maximum heat generation rate. The cumulative heat also increases with the delay of hydration peak and the increase in peak strength.

Because the main hydration peak of SSC mainly corresponds to the formation of hydration products such as ettringite and C-S-H [52]. That is, the main hydration peak contains both silicate reaction and aluminate reaction. Due to the retarding effect of TEA on silicate reaction, the hydration induction period is prolonged, but TEA accelerates aluminate reaction [9,15,17]. Therefore, TEA delays the silicate reaction of slag and accelerates the aluminate reaction of slag at early stage, resulting in the backward delay of the main hydration peak of SSC and the increase in peak strength. Similar to TEA, DEIPA delays the hydration induction period and activates the second reaction of aluminate phase, but its effect is relatively weaker than TEA [24,26]. Therefore, the main hydration peak of SSC

containing DEIPA appears earlier than that of SSC containing TEA. Because the impact of TIPA on the hydration induction period is not apparent [9,20,21], curve collected from isothermal calorimetry about SSC adding TIPA shows a slight delay in its hydration peak. Furthermore, the strength of the main hydration peak of SSC with TIPA changes slightly. The weak effect on the main hydration peak is because TIPA does not greatly promote the hydration of the aluminate phase, which is similar to the results from [53].

3.4. Hydration Products

3.4.1. XRD Analysis

The hydration products of SSC at 3 days and 28 days were analyzed qualitatively and quantitatively by XRD and QXRD to further study the effect of alkanolamine on cement hydration. Figure 6 shows the 3-day and 28-day XRD patterns of SSC with different dosages of TEA, DEIPA and TIPA. Table 5 shows the phase compositions of hardened pastes obtained by Rietveld quantitative analysis. Detailed XRD data is listed in Table S10 of Supplementary Materials and high-resolution pictures are shown in Figures S3 and S4.

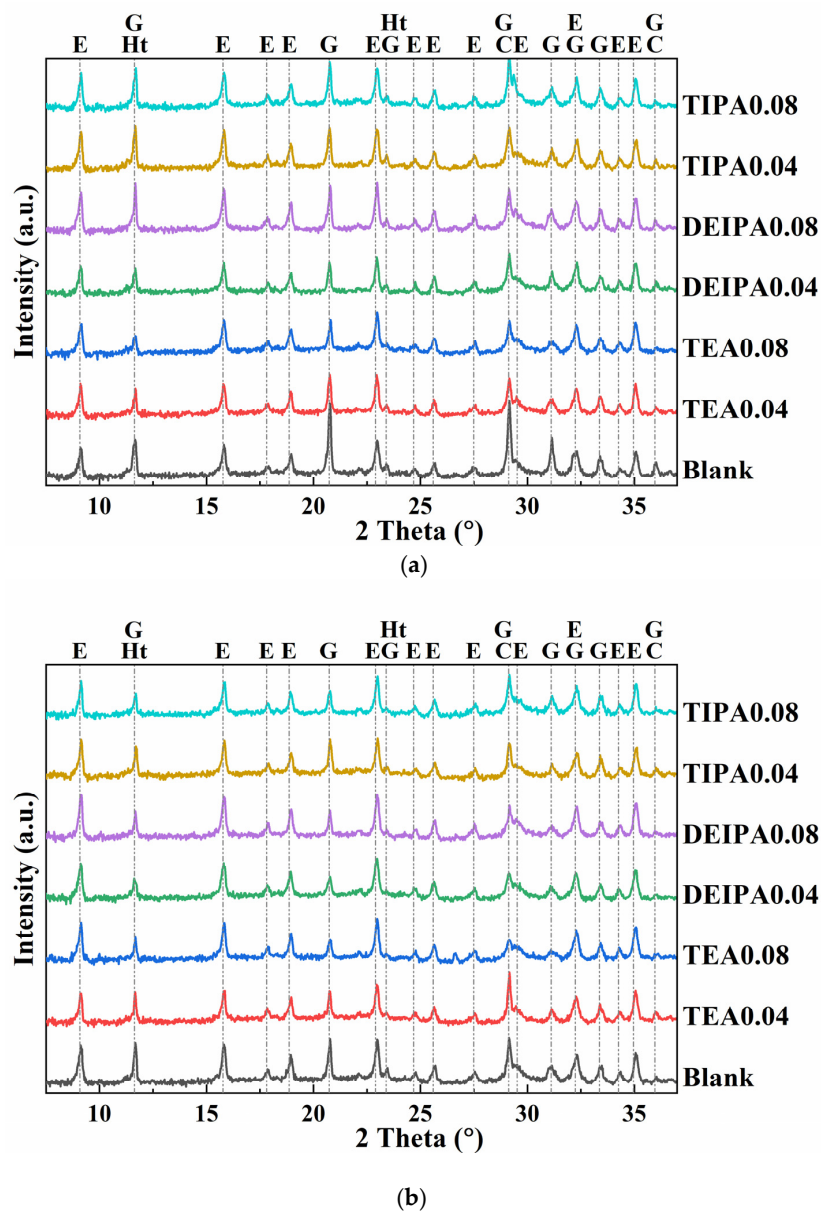


Figure 6. XRD pattern of SSC pastes containing different dosages of alkanolamines (E: Ettringite; G: Gypsum; C: Calcite Ht: Hydrotalcite): (a) 3 d; (b) 28 d.

Table 5. Phase compositions of SSC pastes containing different dosages of alkanolamines as determined by Rietveld analysis.

3 d	Blank	TEA0.04	TEA0.08	DEIPA0.04	DEIPA0.08	TIPA0.04	TIPA0.08
Ettringite	0.1118	0.1162	0.1226	0.1131	0.1343	0.1094	0.1061
Gypsum	0.1115	0.0611	0.0463	0.0529	0.0679	0.0729	0.0747
Calcite	0.0122	0.0075	0.0081	0.0089	0.0060	0.0148	0.0121
Amorphous	0.7644	0.8151	0.8230	0.8091	0.7918	0.8029	0.8071
28 d	Blank	TEA0.04	TEA0.08	DEIPA0.04	DEIPA0.08	TIPA0.04	TIPA0.08
Ettringite	0.1248	0.1259	0.1304	0.1320	0.1407	0.1152	0.1172
Gypsum	0.0700	0.0479	0.0349	0.0421	0.0359	0.0549	0.0477
Calcite	0.0107	0.0112	0.0070	0.0090	0.0089	0.0074	0.0104
Amorphous	0.7945	0.8150	0.8277	0.8170	0.8145	0.8225	0.8247

The main hydration phases of SSC are ettringite, gypsum, and a small amount of calcite due to carbonization. The amorphous humps occurring between 25° and 35° are produced by unhydrated slag [54], and the C-S-H phase cannot be detected by XRD. In addition, as described in [37], because SSC pore solution is undersaturated in monosulphate, no monosulphate is observed in the XRD patterns.

At 3 days, gypsum exists for all mixtures, and relatively obvious ettringite peaks also exist. The strong ettringite peaks of SSC are due to the slag with high Al₂O₃ content used in this experiment. Gypsum content decreases significantly with the addition of alkanolamine, and ettringite content increases correspondingly. The impacts of TEA and DEIPA on SSC are the most significant, followed by TIPA, and the blank is the least significant. The hydration rate of slag is related to the content of gypsum [54]. The greater the gypsum content in SSC, the slower the hydration rate of slag. For TEA and DEIPA, the ettringite content increases correspondingly with the increase in dosage. This agrees with the development of 3-day strength, which also verifies the view that ettringite is responsible for the early strength development of SSC [54].

The calcite content of almost all mixtures is maintained at a low level according to QXRD. The amorphous phase content in the blank sample is lower than that in SSC containing alkanolamines due to the presence of gypsum.

At 28 days, gypsum is further consumed for all mixtures, while the gypsum content in SSC with alkanolamine is still lower than that in the blank sample. The consumption of gypsum by TEA and DEIPA is the most obvious, followed by TIPA. Ettringite content also increases correspondingly, and its enhancement in SSC with DEIPA is the most significant, followed by SSC with TEA, and the worst in SSC with TIPA. Gypsum content decreases and ettringite content increases with the increase in dosage, especially in SSC with DEIPA.

3.4.2. TGA

The TGA results for SSC with different dosages of TEA, DEIPA and TIPA at 3 days and 28 days are shown in Figure 7. Detailed TGA data is listed in Tables S11 and S12 of Supplementary Materials and high-resolution pictures are shown in Figures S5–S10. The thermogravimetric curves shown in Figure 7 indicate the presence of ettringite, gypsum, hydrotalcite and calcite, which agrees with the XRD results. The weight loss of gypsum occurs at approximately 100–150 °C [55,56]. The weight loss of about 100 °C corresponds to the loss of the bound water of ettringite [57–59]. Due to water loss present in the interlayer and dihydroxylation, the C-S-H phase shows weight loss over a wide temperature range of 50–600 °C [50] so that in TGA, it overlaps with ettringite and gypsum. The weight loss of hydrotalcite is usually about 370–400 °C [50,55,60] and overlaps with AFm in TGA [61], but XRD analysis reveals the inadequacy of AFm. Generally speaking, the weight loss peak of portlandite appears at about 400–500 °C, but no corresponding peak can be observed for any of the mixtures. The peak at 700 °C is caused by the decarbonization of CaCO₃ [62]. The weight loss peak of CaCO₃ corresponding to all mixtures is not apparent, indicating

that the carbonization of the hardened pastes is not severe, which is also in good agreement with the result obtained by QXRD. In addition, there is a relatively small weight loss peak at approximately 800 °C, corresponding to the decomposition of C-S-H to wollastonite (CaSiO_3) [63]. By comparing the TGA curves at 3 days and 28 days, it can be seen that the weight loss peak at about 800 °C is enhanced, indicating the formation of the C-S-H phase and its possible contribution to the later strength.

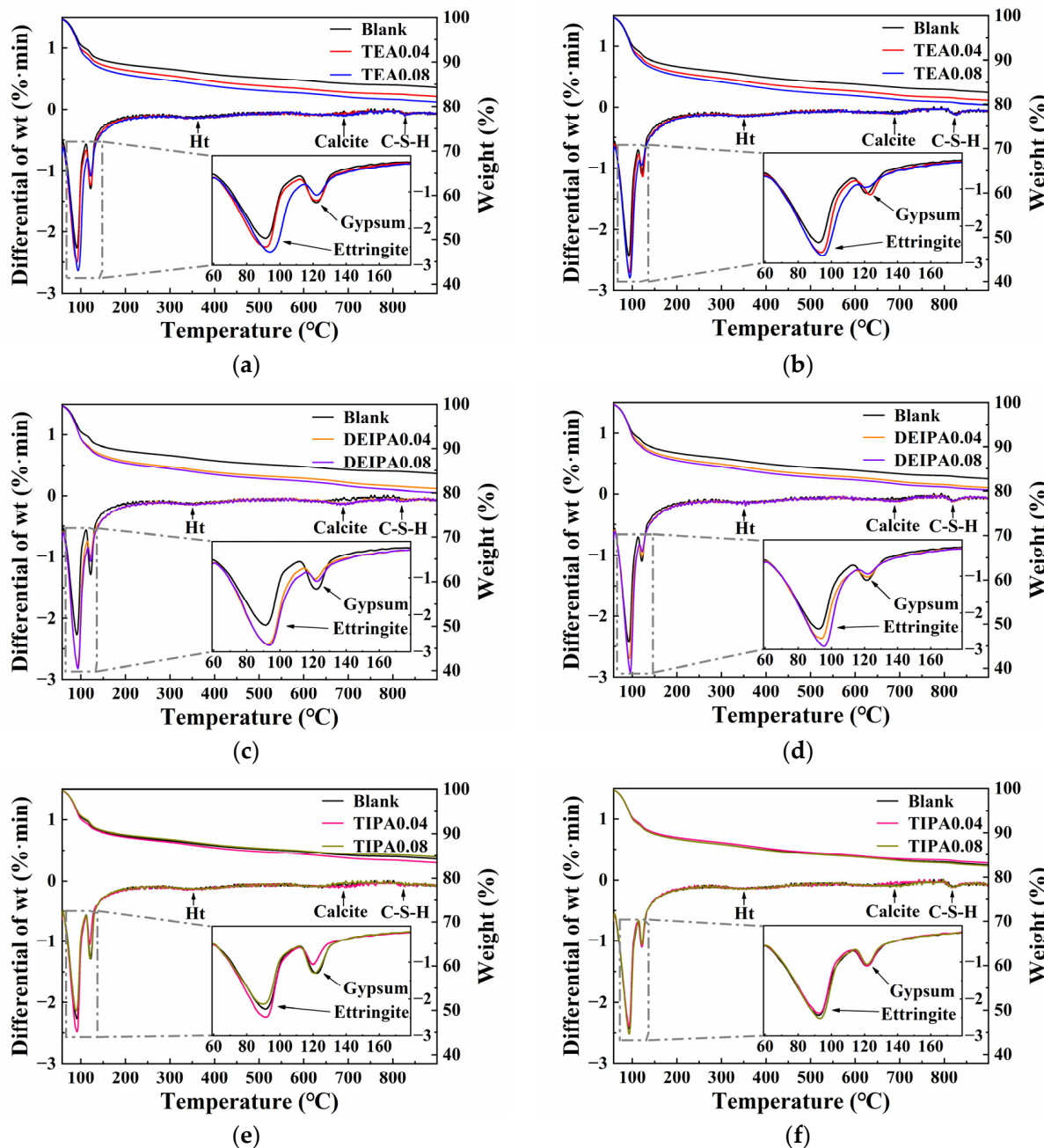


Figure 7. TGA curves of SSC pastes containing different dosages of alkanolamines: (a) TEA 3 d; (b) TEA 28 d; (c) DEIPA 3 d; (d) DEIPA 28 d; (e) TIPA 3 d; (f) TIPA 28 d.

Strong weight loss peaks of ettringite and gypsum can be observed in the TGA curves of all mixtures. Figure 7a,b show that at 3 days, as the dosage of TEA increases, the weight loss peak of ettringite enhances, while the peak of gypsum decreases, which agrees with the XRD results. The total weight loss increases when adding more TEA, which indicates

that TEA promotes the degree of hydration. At 28 days, the peak of ettringite at 0.08% is close to that at 0.04%.

The TGA curve of SSC adding DEIPA is roughly similar to that of SSC adding TEA. What is different is that at 28 days, the ettringite peak in SSC continues to increase when more DEIPA is added. This is because compared with DEIPA, TEA promotes the initial dissolution of slag and the formation of ettringite to a greater extent and blocks the path of ionic dissolution and diffusion at later stages [24]. Therefore, the addition of DEIPA to SSC still results in the formation of new ettringite phase to fill the pore space, which is why DEIPA continues to increase the mechanical properties of SSC in the later stages.

For TIPA, the weight loss peak of ettringite does not increase at 3 days, and even when 0.08% TIPA is added, it is lower than that of the blank sample. Compared with the blank sample, the weight loss peak of gypsum also decreases slightly. At 28 days, TIPA slightly affects ettringite and gypsum, and the total mass loss is not much different from that of the blank sample.

3.5. Morphology

The dosage of each alkanolamine added to SSC samples observed in SEM is 0.08%. The SEM images of the blank sample at 3 days are shown in Figure 8a,b. More ettringite is formed, which agrees with the XRD patterns in Figure 6. This is because the slag with high Al_2O_3 content accelerates the formation of ettringite [54]. As shown in Figure 8a, the surface of most ettringite is covered with C-S-H gel, which has a high density. And some newly formed ettringite has not been covered with C-S-H gel. Pore space for the growth of this kind of ettringite is observed in the upper right corner of Figure 8a, but it is not dense. The more newly formed ettringite, the faster the formation rate of ettringite and the hydration rate of SSC. There are very few hydration products on the surface of gypsum. In contrast, the slag particles located near the gypsum have faster hydration rates, and many hydration products, such as ettringite and C-S-H gel, form nearby. However, there are more angular slag particles far away from the gypsum. Almost no hydration products form on the surface of these slag particles, indicating that many slag particles do not fully participate in the hydration reaction. The SEM images of the blank sample at 28 days are shown in Figure 8c,d. The morphology of SSC becomes denser than that of the sample at 3 days. In addition, almost all slag particles are coated with a large number of hydration products. Columnar ettringite forms and fills pore space, and nearly all ettringite has C-S-H gel attached to its surface.

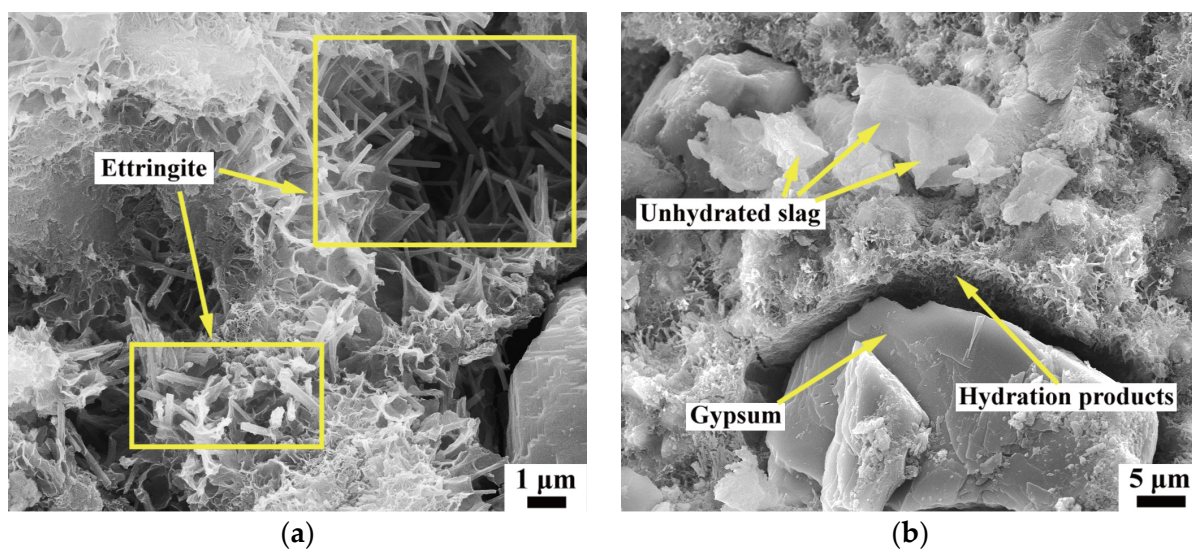


Figure 8. Cont.

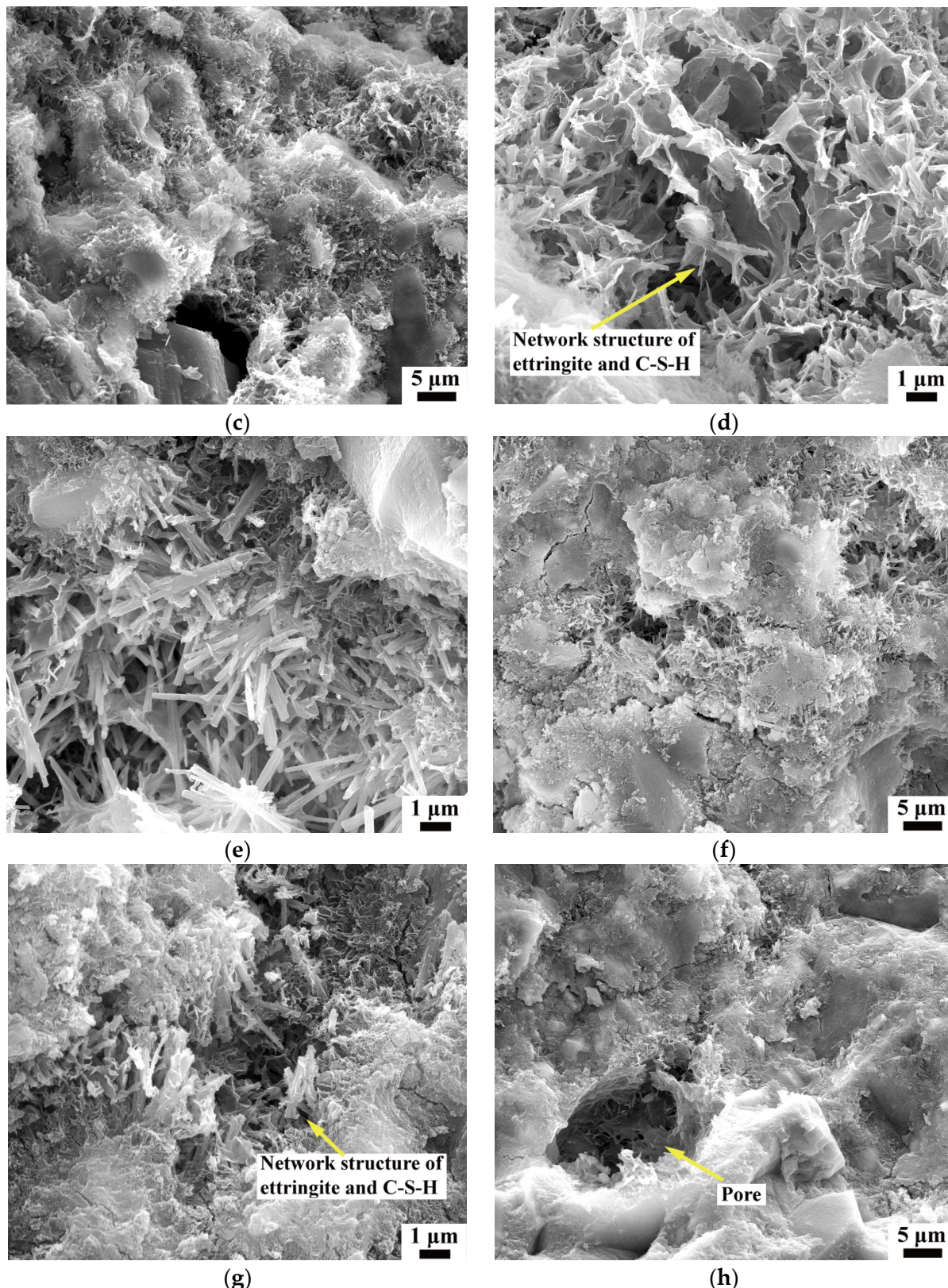


Figure 8. SEM images of the blank sample and SSC adding TEA: (a) Blank 3 d 20,000 \times ; (b) Blank 3 d 5000 \times ; (c) Blank 28 d 5000 \times ; (d) Blank 28 d 20,000 \times ; (e) TEA 3 d 20,000 \times ; (f) TEA 3 d 5000 \times ; (g) TEA 28 d 20,000 \times ; (h) TEA 28 d 5000 \times .

The SEM images of SSC adding TEA at 3 days are shown in Figure 8e,f. A large number of dense columnar ettringite extending outward from the surface of slags is observed. Compared with the blank sample, most of the ettringite is newly formed, and only a tiny part of the ettringite close to slag particles is covered by C-S-H gel. The whole SSC morphology is filled with the extended ettringite, which is denser than that of the blank sample, and particles connect with each other. The SEM images of SSC adding TEA at 28 days are shown in Figure 8g,h. The network structure of ettringite and C-S-H gel covers the entire SSC and the surface of slag is basically covered by hydration products. The morphology is denser, but some large pore space cannot be filled, as seen in Figure 8h.

The SEM images of SSC with DEIPA at 3 days are shown in Figure 9a,b. A large amount of columnar ettringite extends outward and part of the ettringite forms in the pore space. Most slags participate in the hydration reaction and the corresponding hydration products are formed on the surface. The SEM images of SSC with DEIPA at 28 days are shown in Figure 9c,d. The development of 28-day strength caused by DEIPA is evidenced by the coating of hydration products on the surface of slags and the effective filling of pore space crosslinked with ettringite and C-S-H. And large pore space rarely appears.

The SEM image of SSC with TIPA at 3 days is shown in Figure 9e. The surface of ettringite has been covered with C-S-H gel, indicating a slow reaction rate. The SEM image of SSC with TIPA at 28 days is shown in Figure 9f. A dense hydration microstructure like SSC with TEA or DEIPA is not observed.

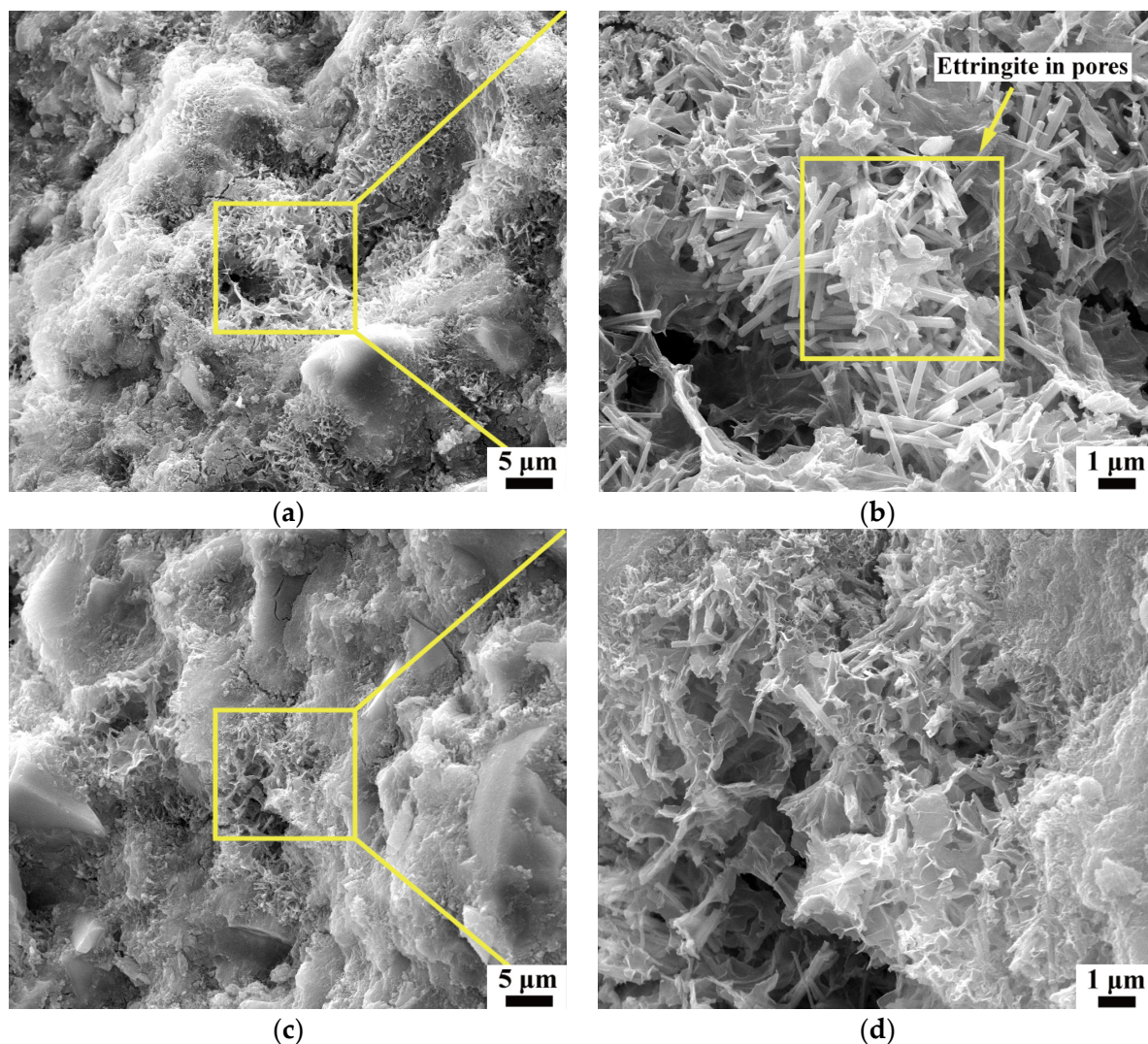


Figure 9. Cont.

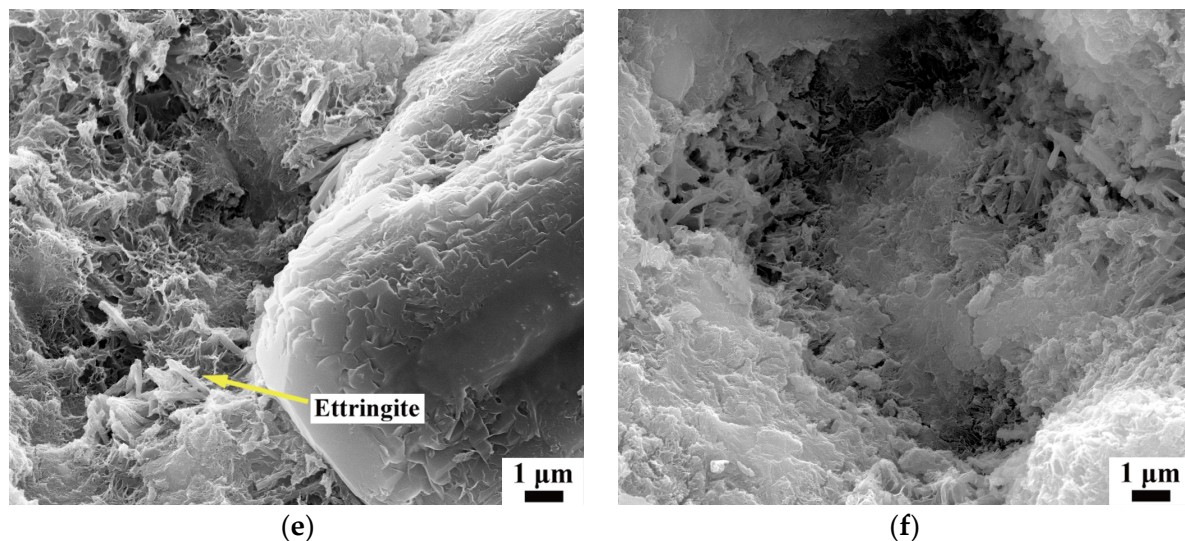


Figure 9. SEM images of SSC adding DEIPA and TIPA: (a) DEIPA 3 d 5000 \times ; (b) DEIPA 3 d 20,000 \times ; (c) DEIPA 28 d 5000 \times ; (d) DEIPA 28 d 20,000 \times ; (e) TIPA 3 d 20,000 \times ; (f) TIPA 28 d 20,000 \times .

4. Discussion

Alkanolamines improve the mechanical properties of low-carbon SSC and increase the hydration degree of slag (as mentioned in Sections 3.1 and 3.2), and the increase in total weight loss also indicates the generation of more hydration products (Figure 7). TEA enhances the early strength of SSC, while DEIPA increases its late strength. The role of TIPA is weak both on early and late strength. It only slightly increases the early strength of SSC at high dosages. TEA plays an important role in SSC at low dosages, while DEIPA tends toward higher dosages. Compared with OPC [9], SSC requires more dosages of TEA and DEIPA so that it can obtain better mechanical properties than OPC, indicating that in a system with high slag content, the potential of alkanolamines for promoting hydration is considerable. The influence of TIPA on SSC is inferior to that on OPC.

According to the results of this study, the corresponding mechanism is discussed (taking TEA as an example as shown in Figure 10). The type of slag affects the growth mechanism of hydration products and the mechanisms are divided into transport controlled dissolution and surface controlled dissolution [36,64]. Slag with Al_2O_3 content below 10 wt.% is defined as low-reactivity slag (LR-slag). Otherwise, it is defined as high-reactivity slag (HR-slag). The Al_2O_3 content of slag used in this study is HR-slag, which contains 17.7 wt.% Al_2O_3 . The surface of slag has a fast dissolution reaction, so transport controlled dissolution is the main dissolution mechanism on slag surface. The dissolution of slag is limited by the rate of diffusion of dissolved products and the formation of the concentration gradient.

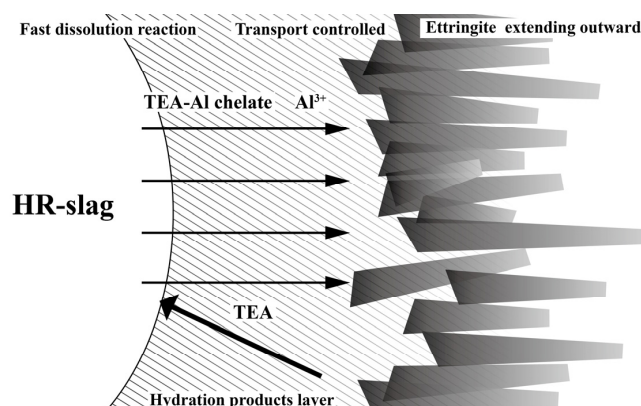
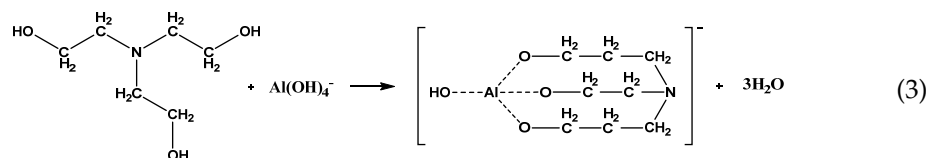


Figure 10. Hydration scheme for the hardening of SSC adding TEA.

Hydration heat analysis and phase analysis show that the inclusion of TEA does promote the aluminate reaction of SSC and the formation of ettringite, which is related to the chelation of TEA with metal ions. TEA chelates with Al^{3+} ions in the cement hydration process, as demonstrated in Equation (3) [11,65,66]:



TEA forms TEA-Al chelate compound by chelating with Al^{3+} ions, which accelerates the dissolution of Al^{3+} ions. The chelate transports Al^{3+} ions dissolved on slag surface outside the slag particles, thereby improving the diffusion efficiency of Al^{3+} ions. This process has two effects on the hydration of SSC: (i) it reduces the concentration gradient on slag surface, resulting in the formation of columnar ettringite that extends outward into the pore space; (ii) the increase in diffusion efficiency also accelerates the dissolution of slag itself, resulting in the improvement of the hydration degree of slag. The greater amount of newly formed columnar ettringite in Figure 8e than in Figure 8a is evidence that TEA promotes the outward diffusion of Al^{3+} ions to reduce the ion concentration gradient on slag surface. The columnar ettringite formed in the pore space is covered by C-S-H gel at later stages, which plays an essential role in the strength development of SSC.

Figure 11 shows the hydration scheme of alkanolamine added to SSC. According to the experimental analysis of [15], TEA accelerates the initial dissolution of gypsum and aluminate phase and promotes the initial precipitation of ettringite. In other words, TEA accelerates the formation of hydration products on the surface of slag during initial hydration. If the hydration product formed at this time is too dense, it will block the path of further dissolution and migration of ions, affecting the hydration of SSC. Therefore, appropriate dosage is critical. More is not always better. According to the analysis of Figures 3 and 4, when the dosage of TEA reaches 0.04–0.06%, the mechanical properties and hydration degree of SSC reach the maximum value. The morphology of Figure 8h also finds unfilled pore space at high content. The first peak of initial hydration is lower for the sample with the addition of DEIPA than that with TEA [24]. In this study, the heat of hydration of DEIPA at 3 days is also lower than that of TEA. This indicates that the promoting effect of DEIPA on initial hydration of SSC is not as strong as that of TEA, so DEIPA can still improve the mechanical properties of SSC at high dosages.

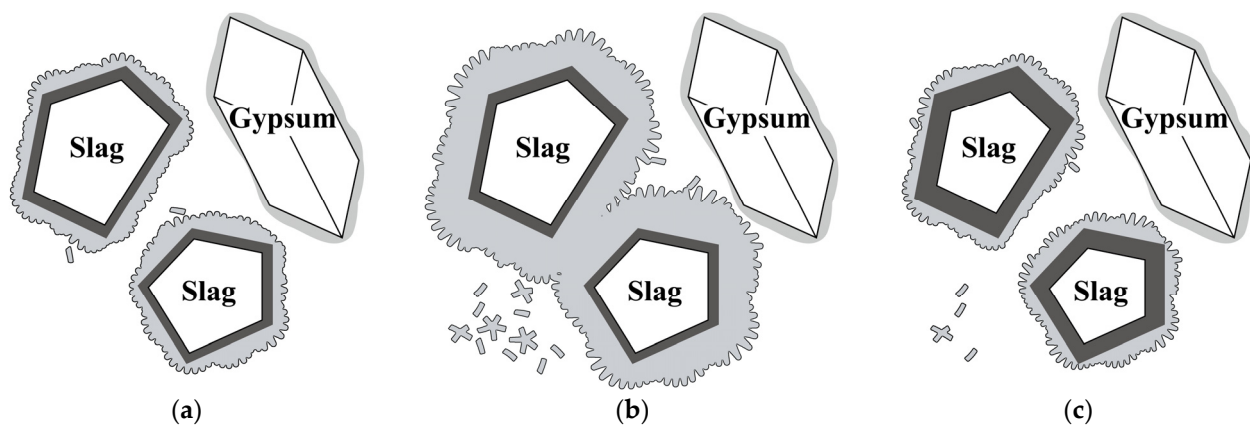


Figure 11. Hydration scheme of SSC adding alkanolamines (light gray represents the hydration products extending outward, while dark gray represents the dense hydration products layer): (a) without alkanolamines (formation of small amounts of hydration products); (b) appropriate dosage (formation of a large amount of hydration products); (c) excessive dosage (dense hydration products layer inhibiting further hydration).

Why TEA and DEIPA can still increase the 28-day strength of SSC is related to the lack of adsorption effect of AFm on alkanolamine. In Portland cement, TEA is removed by AFm after the sulfate exhaustion point due to low steric hindrance [15,19] and DEIPA also has a similar effect [24]. However, at 28 days, although gypsum content greatly decreases for all mixtures, the obvious gypsum peak still exists. When the content of gypsum is sufficient, it is difficult to convert AFt to AFm so that AFm peaks in XRD or TGA cannot be seen. Therefore, due to the lack of the adsorption effect of AFm on TEA and DEIPA, they continue to increase the late strength of SSC.

The influence of TIPA on the mechanical properties of SSC is weak because compared with its strong effect on the dissolution of Fe^{3+} , TIPA is not so good at accelerating the dissolution of Al^{3+} and Si^{4+} ions [19,20]. And the Fe_2O_3 content of slag used in SSC is insufficient. This is disadvantageous to SSC, a system with ettringite responsible for the early strength development. The hydration heat analysis in Figure 5 also proves this point. In addition, due to the influence of air-entraining effect [9,21,67], TIPA cannot enhance the early and late strength of SSC.

Three alkanolamines (TEA, DEIPA, and TIPA) have similar chemical formulas. Their chelation with metal ions is mainly attributed to the coordination bond formed by -OH and metal ions, and the coordination bond between N and metal ions is relatively weak [11,16,23]. The three alkanolamines in the order of left to right, the number of -CH₃ groups increases in order, and the relative molecular mass increases in order. The role of alkanolamines on improving the maximum heat generation rate of the main hydration peak: TEA > DEIPA > TIPA (Figure 5). Therefore, -CH₃ interferes with the coordination between -OH and metal ions, affecting the chelation of alkanolamine with metal ions.

In short, alkanolamines such as TEA and DEIPA can effectively increase the strength of low-carbon SSC by nearly 50% through the chelating effect, indicating the potential application of SSC as a material with low environmental pollution in construction engineering.

5. Conclusions

In this work, the effects of three alkanolamines on cement hydration and strength development in SSC system were investigated using the combined techniques of calorimetry, XRD, TGA and SEM. The hydration mechanism of alkanolamines on SSC was demonstrated. The following conclusions can be drawn.

TEA and DEIPA significantly increase the compressive strength of SSC. The two have different preferences, with TEA tending towards earlier stages and DEIPA tending towards later stages. TEA is better at low dosages, while DEIPA is more suitable at high dosages. The influence of TIPA on the early strength of SSC is weak and TIPA is harmful to the late strength of SSC. Compared with OPC, SSC needs to add more dosages of alkanolamine to achieve better strength development. This is a potential and effective way to improve the strength of SSC.

TEA and DEIPA accelerate the dissolution of slag at early stage, promote its aluminate reaction, and consume a large amount of gypsum, which leads to the formation of more hydration products such as ettringite, resulting in early strength improvement. The acceleration of slag dissolution is attributed to the chelation of alkanolamine with Al^{3+} ions. -CH₃ in alkanolamine interferes with the coordination between -OH and metal ions. So alkanolamine with more -CH₃ has a weaker chelating effect with Al^{3+} ions, thus inhibiting early hydration and strength development.

Above all, alkanolamine plays a more important role in SSC than OPC. And alkanolamines also differ from each other greatly due to different groups. This study did not provide an in-depth experimental exploration of the ion chelating effect of alkanolamine on SSC. The role of different groups in different molecules in hydration needs to be further explained. This may require relevant experiments such as ¹H-NMR and FTIR. In addition, SSC is a system very sensitive to alkalinity, and its mechanical properties are also related to the complexity of the chemical composition of the slag influencing its solubility. There-

fore, more in-depth discussions of the effect of alkanolamine on SSC with different clinker content and slag types are needed in the future.

Supplementary Materials: The following supporting information can be downloaded at: <https://www.mdpi.com/article/10.3390/su16073008/s1>, Table S1: Compressive strength; Table S2: Detailed compressive strength data of SSC adding TEA at 3 d; Table S3: Detailed compressive strength data of SSC adding TEA at 28 d; Table S4: Detailed compressive strength data of SSC adding DEIPA at 3 d; Table S5: Detailed compressive strength data of SSC adding DEIPA at 28 d; Table S6: Detailed compressive strength data of SSC adding TIPA at 3 d; Table S7: Detailed compressive strength data of SSC adding TIPA at 28 d; Table S8: Hydration degree; Table S9: Hydration heat; Table S10: XRD; Table S11: TGA (Differential); Table S12: TGA (integral); Figure S1: High-resolution pictures of Figure 5a; Figure S2: High-resolution pictures of Figure 5b; Figure S3: High-resolution pictures of Figure 6a; Figure S4: High-resolution pictures of Figure 6b; Figure S5: High-resolution pictures of Figure 7a; Figure S6: High-resolution pictures of Figure 7b; Figure S7: High-resolution pictures of Figure 7c; Figure S8: High-resolution pictures of Figure 7d; Figure S9: High-resolution pictures of Figure 7e; Figure S10: High-resolution pictures of Figure 7f.

Author Contributions: Conceptualization, R.Z. and H.C. and B.J.; methodology, R.Z. and H.C. and S.W.; software, R.Z.; validation, R.Z. and H.C.; formal analysis, R.Z.; investigation, R.Z.; resources, R.Z.; data curation, R.Z.; writing—original draft preparation, R.Z.; writing—review and editing, R.Z. and H.C. and S.F.; visualization, R.Z. and H.C.; supervision, H.C. and S.F. and F.H.; project administration, H.C.; funding acquisition, H.C. All authors have read and agreed to the published version of the manuscript.

Funding: This research was funded by Sichuan Province Science and Technology Plan Project, grant number 2023YFSY0019.

Institutional Review Board Statement: Not applicable.

Informed Consent Statement: Not applicable.

Data Availability Statement: The data presented in this study are not available due to privacy.

Conflicts of Interest: Authors Shu-Jing Fan and Fa-Fu Hang were employed by Linhai Zhongxin New Building Materials Co., Ltd. The remaining authors declare that the research was conducted in the absence of any commercial or financial relationships that could be construed as a potential conflict of interest.

References

1. Hafez, H.; Kassim, D.; Kurda, R.; Silva, R.V.; de Brito, J. Assessing the sustainability potential of alkali-activated concrete from electric arc furnace slag using the ECO₂ framework. *Constr. Build. Mater.* **2021**, *281*, 122559. [[CrossRef](#)]
2. Shahane, H.A.; Patel, S. Influence of curing method on characteristics of environment-friendly angular shaped cold bonded fly ash aggregates. *J. Build. Eng.* **2021**, *35*, 101997. [[CrossRef](#)]
3. Scrivener, K.L.; John, V.M.; Gartner, E.M. Eco-efficient cements: Potential economically viable solutions for a low-CO₂ cement-based materials industry. *Cem. Concr. Res.* **2018**, *114*, 2–26. [[CrossRef](#)]
4. Schneider, M.; Romer, M.; Tschudin, M.; Bolio, H. Sustainable cement production—Present and future. *Cem. Concr. Res.* **2011**, *41*, 642–650. [[CrossRef](#)]
5. Trung, N.T.; Alemi, N.; Haido, J.H.; Shariati, M.; Baradaran, S.; Yousif, S.T. Reduction of cement consumption by producing smart green concretes with natural zeolites. *Smart Struct. Syst.* **2019**, *24*, 415–425. [[CrossRef](#)]
6. He, Y.; Liu, S.; Hooton, R.D.; Zhang, X.; He, S. Effects of TEA on rheological property and hydration performance of lithium slag-cement composite binder. *Constr. Build. Mater.* **2022**, *318*, 125757. [[CrossRef](#)]
7. Kong, X.-M.; Lu, Z.-B.; Liu, H.; Wang, D.-M. Influence of triethanolamine on the hydration and the strength development of cementitious systems. *Mag. Concr. Res.* **2013**, *65*, 1101–1109. [[CrossRef](#)]
8. Xu, Z.; Li, W.; Sun, J.; Hu, Y.; Xu, K.; Ma, S.; Shen, X. Hydration of Portland cement with alkanolamines by thermal analysis. *J. Therm. Anal. Calorim.* **2017**, *131*, 37–47. [[CrossRef](#)]
9. Xu, Z.; Li, W.; Sun, J.; Hu, Y.; Xu, K.; Ma, S.; Shen, X. Research on cement hydration and hardening with different alkanolamines. *Constr. Build. Mater.* **2017**, *141*, 296–306. [[CrossRef](#)]
10. Zhang, Y.; Gao, L.; Cai, X.; Li, Q.; Kong, X. Influences of triethanolamine on the performance of cement pastes used in slab track. *Constr. Build. Mater.* **2020**, *238*, 117670. [[CrossRef](#)]
11. Yaphary, Y.L.; Yu, Z.; Lam, R.H.W.; Lau, D. Effect of triethanolamine on cement hydration toward initial setting time. *Constr. Build. Mater.* **2017**, *141*, 94–103. [[CrossRef](#)]

12. Perez, J.-P.; Nonat, A.; Garrault, S.; Pourchet, S.; Mosquet, M. Influence of triisopropanolamine on the physico-chemical and mechanical properties of pure cement pastes and mortars. In Proceedings of the 11th ICCC, Durban, South Africa, 11–16 May 2003; Volume 28, pp. 454–463.
13. Ramachandran, V.S. Action of triethanolamine on the hydration of tricalcium aluminate. *Cem. Concr. Res.* **1973**, *3*, 41–54. [\[CrossRef\]](#)
14. Han, J.; Wang, K.; Shi, J.; Wang, Y. Mechanism of triethanolamine on Portland cement hydration process and microstructure characteristics. *Constr. Build. Mater.* **2015**, *93*, 457–462. [\[CrossRef\]](#)
15. Lu, Z.; Kong, X.; Jansen, D.; Zhang, C.; Wang, J.; Pang, X.; Yin, J. Towards a further understanding of cement hydration in the presence of triethanolamine. *Cem. Concr. Res.* **2020**, *132*, 106041. [\[CrossRef\]](#)
16. Yan-Rong, Z.; Xiang-Ming, K.; Zi-Chen, L.; Zhen-Bao, L.; Qing, Z.; Bi-Qin, D.; Feng, X. Influence of triethanolamine on the hydration product of portlandite in cement paste and the mechanism. *Cem. Concr. Res.* **2016**, *87*, 64–76. [\[CrossRef\]](#)
17. He, Y.; Liu, S.; Zhang, X.; Liu, W.; Liao, G.; Xu, M. Influence of triethanolamine on mechanical strength and hydration performance of blended cement containing fly ash, limestone and slag. *J. Build. Eng.* **2021**, *44*, 102879. [\[CrossRef\]](#)
18. Sandberg, P.J.; Doncaster, F. On the mechanism of strength enhancement of cement paste and mortar with triisopropanolamine. *Cem. Concr. Res.* **2004**, *34*, 973–976. [\[CrossRef\]](#)
19. Gartner, E.; Myers, D. Influence of tertiary alkanolamines on portland-cement hydration. *J. Am. Ceram. Soc.* **1993**, *76*, 1521–1530. [\[CrossRef\]](#)
20. Huang, H.; Li, X.-r.; Shen, X.-d. Hydration of ternary cement in the presence of triisopropanolamine. *Constr. Build. Mater.* **2016**, *111*, 513–521. [\[CrossRef\]](#)
21. Ma, B.; Zhang, T.; Tan, H.; Liu, X.; Mei, J.; Qi, H.; Jiang, W.; Zou, F. Effect of triisopropanolamine on compressive strength and hydration of cement-fly ash paste. *Constr. Build. Mater.* **2018**, *179*, 89–99. [\[CrossRef\]](#)
22. Zhang, F.; Bai, Y.; Cai, Y.; Chen, B.; Ning, F. Effect of Triisopropanolamine on the Compressive Strength and Early Hydration of Cement at Low Temperature. *J. Wuhan Univ. Technol.-Mater. Sci. Ed.* **2020**, *35*, 611–619. [\[CrossRef\]](#)
23. Wang, J.; Chang, L.; Yue, D.; Zhou, Y.; Liu, H.; Wang, Y.; Yang, S.; Cui, S. Effect of chelating solubilization via different alkanolamines on the dissolution properties of steel slag. *J. Clean. Prod.* **2022**, *365*, 132824. [\[CrossRef\]](#)
24. Lu, Z.; Kong, X.; Jansen, D.; Zhang, C. A comparative study of the effects of two alkanolamines on cement hydration. *Adv. Cem. Res.* **2022**, *34*, 47–56. [\[CrossRef\]](#)
25. Wang, Y.; Lei, L.; Hu, X.; Liu, Y.; Shi, C. Effect of diethanolisopropanolamine and ethyldiisopropylamine on hydration and strength development of Portland cement. *Cem. Concr. Res.* **2022**, *162*, 132824. [\[CrossRef\]](#)
26. Ma, S.; Li, W.; Zhang, S.; Hu, Y.; Shen, X. Study on the hydration and microstructure of Portland cement containing diethanol-isopropanolamine. *Cem. Concr. Res.* **2015**, *67*, 122–130. [\[CrossRef\]](#)
27. Lu, X.; Ye, Z.; Zhang, L.; Hou, P.; Cheng, X. The influence of ethanol-diisopropylamine on the hydration and mechanical properties of Portland cement. *Constr. Build. Mater.* **2017**, *135*, 484–489. [\[CrossRef\]](#)
28. Heinz, D.; Göbel, M.; Hilbig, H.; Urbonas, L.; Bujauskaite, G. Effect of TEA on fly ash solubility and early age strength of mortar. *Cem. Concr. Res.* **2010**, *40*, 392–397. [\[CrossRef\]](#)
29. Riding, K.; Silva, D.A.; Scrivener, K. Early age strength enhancement of blended cement systems by CaCl_2 and diethanol-isopropanolamine. *Cem. Concr. Res.* **2010**, *40*, 935–946. [\[CrossRef\]](#)
30. Juenger, M.C.G.; Winnefeld, F.; Provis, J.L.; Ideker, J.H. Advances in alternative cementitious binders. *Cem. Concr. Res.* **2011**, *41*, 1232–1243. [\[CrossRef\]](#)
31. Novak, R.; Schneider, W.; Lang, E. New knowledge regarding the supersulphated cement Slagstar. *ZKG Int.* **2005**, *58*, 70–78.
32. Dutta, D.K.; Borthakur, P.C. Activation of low lime high alumina granulated blast-furnace slag by anhydrite. *Cem. Concr. Res.* **1990**, *20*, 711–722. [\[CrossRef\]](#)
33. Bijen, J.; Niel, E. Supersulfated cement from blastfurnace slag and chemical gypsum available in the netherlands and neighboring countries. *Cem. Concr. Res.* **1981**, *11*, 307–320. [\[CrossRef\]](#)
34. Gruskovnjak, A.; Lothenbach, B.; Winnefeld, F.; Münch, B.; Figi, R.; Ko, S.-C.; Adler, M.; Mäder, U. Quantification of hydration phases in supersulfated cements: Review and new approaches. *Adv. Cem. Res.* **2011**, *23*, 265–275. [\[CrossRef\]](#)
35. Rubert, S.; Angulski da Luz, C.; Varela, M.V.F.; Pereira Filho, J.I.; Hooton, R.D. Hydration mechanisms of supersulfated cement. *J. Therm. Anal. Calorim.* **2018**, *134*, 971–980. [\[CrossRef\]](#)
36. Gruskovnjak, A.; Lothenbach, B.; Winnefeld, F.; Figi, R.; Ko, S.C.; Adler, M.; Mäder, U. Hydration mechanisms of super sulphated slag cement. *Cem. Concr. Res.* **2008**, *38*, 983–992. [\[CrossRef\]](#)
37. Matschei, T.; Bellmann, E.; Stark, J. Hydration behaviour of sulphate-activated slag cements. *Adv. Cem. Res.* **2005**, *17*, 167–178. [\[CrossRef\]](#)
38. Grounds, T.; Nowell, D.V.; Wilburn, F.W. The influence of temperature and different storage-conditions on the stability of supersulphated cement. *J. Therm. Anal.* **1994**, *41*, 687–699. [\[CrossRef\]](#)
39. Erdem, E.; Olmez, H. The mechanical-properties of supersulphated cement containing phosphogypsum. *Cem. Concr. Res.* **1993**, *23*, 115–121. [\[CrossRef\]](#)
40. Grounds, T.; Nowell, D.V.; Wilburn, F.W. Resistance of supersulfated cement to strong sulfate solutions. *J. Therm. Anal. Calorim.* **2003**, *72*, 181–190. [\[CrossRef\]](#)

41. Pinto, S.R.; da Luz, C.A.; Munhoz, G.S.; Medeiros, R.A. Durability of phosphogypsum-based supersulfated cement mortar against external attack by sodium and magnesium sulfate. *Cem. Concr. Res.* **2020**, *136*, 106172. [[CrossRef](#)]
42. Pinto, S.R.; da Luz, C.A.; Munhoz, G.S.; Medeiros-Junior, R.A. Resistance of phosphogypsum-based supersulfated cement to carbonation and chloride ingress. *Constr. Build. Mater.* **2020**, *263*, 120640. [[CrossRef](#)]
43. Cabrera-Luna, K.; Perez-Cortes, P.; Garcia, I.E. Pumice-based supersulfated cements in mortars: Effects of pumice fineness and activator ratio on physical and environmental characteristics. *Constr. Build. Mater.* **2022**, *342*, 127947. [[CrossRef](#)]
44. Goetz-Neunhoeffer, F.; Neubauer, J. Refined ettringite ($\text{Ca}_6\text{Al}_2(\text{SO}_4)_3(\text{OH})_{12} \bullet 26\text{H}_2\text{O}$) structure for quantitative X-ray diffraction analysis. *Powder Diffr.* **2006**, *21*, 4–11. [[CrossRef](#)]
45. Boeyens, J.C.A.; Ichharam, V.V.H. Redetermination of the crystal structure of calcium sulphate dihydrate, $\text{CaSO}_4 \bullet 2\text{H}_2\text{O}$. *Z. Fur Krist.-New Cryst. Struct.* **2002**, *217*, 9–10. [[CrossRef](#)]
46. Markgraf, S.A.; Reeder, R.J. High-temperature structure refinements of calcite and magnesite. *Am. Mineral.* **1985**, *70*, 590–600.
47. Burdett, J.K.; Hughbanks, T.; Miller, G.J.; Richardson, J.W., Jr.; Smith, J.V. Structural-electronic relationships in inorganic solids: Powder neutron diffraction studies of the rutile and anatase polymorphs of titanium dioxide at 15 and 295 K. *J. Am. Chem. Soc.* **1987**, *109*, 3639–3646. [[CrossRef](#)]
48. Kocabas, V.; Gallucci, E.; Scrivener, K.L. Methods for determination of degree of reaction of slag in blended cement pastes. *Cem. Concr. Res.* **2012**, *42*, 511–525. [[CrossRef](#)]
49. Luke, K.; Glasser, F.P. Selective dissolution of hydrated blast-furnace slag cements. *Cem. Concr. Res.* **1987**, *17*, 273–282. [[CrossRef](#)]
50. Taylor, H.F.W. *Cement Chemistry*, 2nd ed.; Thomas Telford: London, UK, 1997. [[CrossRef](#)]
51. Wang, Y.; Hu, Y.; He, X.; Su, Y.; Strnadel, B.; Miao, W. Hydration and compressive strength of supersulfated cement with low-activity high alumina ferronickel slag. *Cem. Concr. Compos.* **2023**, *136*, 104892. [[CrossRef](#)]
52. Bazaldua-Medellin, M.E.; Fuentes, A.F.; Gorokhovsky, A.; Escalante-Garcia, J.I. Early and late hydration of supersulphated cements of blast furnace slag with fluorgypsum. *Mater. De Constr.* **2015**, *65*, e043. [[CrossRef](#)]
53. Tan, H.; Nie, K.; He, X.; Guo, Y.; Zhang, X.; Deng, X.; Su, Y.; Yang, J. Effect of organic alkali on compressive strength and hydration of wet-grinded granulated blast-furnace slag containing Portland cement. *Constr. Build. Mater.* **2019**, *206*, 10–18. [[CrossRef](#)]
54. Masoudi, R.; Hooton, R.D. Examining the hydration mechanism of supersulfated cements made with high and low-alumina slags. *Cem. Concr. Compos.* **2019**, *103*, 193–203. [[CrossRef](#)]
55. Lothenbach, B.; Durdziński, P.; De Weerdt, K. Thermogravimetric analysis. In *A Practical Guide to Microstructural Analysis of Cementitious Materials*; Scrivener, K., Snellings, R., Lothenbach, B., Eds.; CRC Press: Boca Raton, FL, USA, 2016; pp. 178–208.
56. Cassagnabere, F.; Mouret, M.; Escadeillas, G. Early hydration of clinker-slag-metakaolin combination in steam curing conditions, relation with mechanical properties. *Cem. Concr. Res.* **2009**, *39*, 1164–1173. [[CrossRef](#)]
57. Kalpokaite-Dickuviene, R.; Baltusnikas, A.; Levinskas, R.; Cesniene, J. Incinerator residual ash-metakaolin blended cements: Effect on cement hydration and properties. *Constr. Build. Mater.* **2019**, *206*, 297–306. [[CrossRef](#)]
58. Wang, S.D.; Scrivener, K.L. Hydration products of alkali-activated slag cement. *Cem. Concr. Res.* **1995**, *25*, 561–571. [[CrossRef](#)]
59. Angulo-Ramirez, D.E.; de Gutierrez, R.M.; Puertas, F. Alkali-activated Portland blast-furnace slag cement: Mechanical properties and hydration. *Constr. Build. Mater.* **2017**, *140*, 119–128. [[CrossRef](#)]
60. Nied, D.; Enemark-Rasmussen, K.; L'Hopital, E.; Skibsted, J.; Lothenbach, B. Properties of magnesium silicate hydrates (M-S-H). *Cem. Concr. Res.* **2016**, *79*, 323–332. [[CrossRef](#)]
61. Nguyen, H.A.; Chang, T.P.; Shih, J.Y.; Chen, C.T. Influence of low calcium fly ash on compressive strength and hydration product of low energy super sulfated cement paste. *Cem. Concr. Compos.* **2019**, *99*, 40–48. [[CrossRef](#)]
62. Xing, J.; Zhou, Y.; Peng, Z.; Wang, J.; Jin, Y.; Jin, M. The influence of different kinds of weak acid salts on the macro-performance, micro-structure, and hydration mechanism of the supersulfated cement. *J. Build. Eng.* **2023**, *66*, 105937. [[CrossRef](#)]
63. Li, Y.; Qiao, C.Y.; Ni, W. Green concrete with ground granulated blast-furnace slag activated by desulfurization gypsum and electric arc furnace reducing slag. *J. Clean. Prod.* **2020**, *269*, 122212. [[CrossRef](#)]
64. Stumm, W.; Morgan, J.J. *Aquatic Chemistry*, 3rd ed.; John Wiley & Sons Inc.: Hoboken, NJ, USA, 1996; Volume 25, p. 1162.
65. Pinkas, J.; Verkade, J.G. Alumatrane, $\text{Al}(\text{OCH}_2\text{CH}_2)_3\text{N}$: A reinvestigation of its oligomeric behavior. *Inorg. Chem.* **1993**, *32*, 2711–2716. [[CrossRef](#)]
66. Fernandez, L.; Viruela-Martín, P.; Latorre, J.; Guillem, C.; Beltrán, A.; Amorós, P. Theoretical study of oligomeric alumatranes present in the chemistry of materials from micro to mesoporous molecular sieves and alumina composites. *J. Mol. Struct.* **2008**, *850*, 94–104. [[CrossRef](#)]
67. Huang, H.; Li, X.; Avet, F.; Hanpongmun, W.; Scrivener, K. Strength-promoting mechanism of alkanolamines on limestone-calcined clay cement and the role of sulfate. *Cem. Concr. Res.* **2021**, *147*, 106527. [[CrossRef](#)]

Disclaimer/Publisher's Note: The statements, opinions and data contained in all publications are solely those of the individual author(s) and contributor(s) and not of MDPI and/or the editor(s). MDPI and/or the editor(s) disclaim responsibility for any injury to people or property resulting from any ideas, methods, instructions or products referred to in the content.